CIRP Journal of Manufacturing Science and Technology 49 (2024) 14–27

Contents lists available at ScienceDirect

CIRP Journal of Manufacturing Science and Technology

journal homepage: www.elsevier.com/locate/cirpj

Charge weld evolution in hollow aluminum extrusion: Experiments and modeling

Eren Can Sariyarlioglu [a], Marco Negozio [b], Torgeir Welo [a], Jun Ma [a,*]

[a] Department of Mechanical and Industrial Engineering, Norwegian University of Science and Technology, Trondheim 7491, Norway
[b] Department of Engineering and Architecture, University of Parma, Parma 43124, Italy

ARTICLE INFO

Keywords:
Aluminum extrusion
Charge weld
Transverse weld
Front-end defect
Scrap minimization

ABSTRACT

Charge welds occur in billet-to-billet extrusion processes due to the transition between successive billets. The material in this transition zone is typically characterized by substandard mechanical properties. In industrial practice, a specified length of the extruded profile is cut away and recycled as in-process scrap. Therefore, understanding the extrusion mechanisms affecting the properties of the charge weld is crucial to controlling product quality, reducing non-conformities and improving the extrusion yield. This paper provides new insights into thermo-mechanical mechanisms associated with charge weld of circular aluminum tubes. A large number of carefully-controlled, full-scale extrusion experiments were conducted in an industrial environment to research charge weld evolution mechanisms and influential parameters. In addition, a finite element (FE) model was developed to predict the charge weld evolution across the cross section and along the profile. The experimental and numerical results show good agreement in terms of the location of the charge weld within the extruded profile. Moreover, a comparison with analytical models in the literature reveals that the FE model provides a significantly more accurate prediction of the length of the extruded profile affected by the charge weld ('scrap length'). Based on the validated FE model, a sensitivity study was done to explore the effect of process parameters on charge weld evolution, particularly focusing on material flow and dead metal zone. The results show that the ram speed influences the charge weld evolution, while changes in billet temperature are insignificant. In conclusion, the findings presented in this study provide new insights that serve as practical guidance to the mechanism of charge weld evolution. They also highlight the applicability and limitations of numerical and analytical methods in assessing industrial extrusion problems.

1. Introduction

Aluminum extrusion has emerged as an efficient method to produce a wide array of products, ranging from rods, bars, and tubes to complex cross-sectional designs, presenting a competitive advantage in the manufacturing of lightweight products [6]. However, a survey carried out by the European Aluminum Association (EAA) with 69 extruders shows that as much as 22–24% of the billet material is scrapped in the extrusion process [22]. Therefore, reducing in-process scrap is crucial for increasing extrusion yield, thus improving process efficiency and promoting sustainability. Charge weld is one of the most important sources to in-process scrap, along with seam weld (longitudinal weld) and billet skin contamination (back-end defect), which can potentially degrade the properties of the product [27]. Charge welds are unavoidable during billet-to-billet extrusion and their presence can degrade the mechanical integrity of extruded profiles.

In principle, the charge weld is a solid-state pressure weld that forms from the transition zone in the extruded profile during billet-to-billet extrusion and the continuous flow between the successive billets. As shown in Fig. 1, after a press stroke is completed, the die remains filled with the material from the previous billet ('old billet'). During the waiting time for the next press stroke to begin, a stop mark appears on the extrudate. It is caused by material sticking to the bearing surface of the die, indicating the transition between two process strokes. When a new billet is loaded into the container and the extrusion process starts, the back surface of the old billet starts interacting with the new billet. Ideally, if the merging surfaces of both billets were perfectly clean without the presence of any aluminium oxide layer, and had the same mechanical properties, this configuration could be considered non-defective [31]. In practice, however, the butt-ends are oxidized, and

* Corresponding author.
E-mail address: jun.ma@ntnu.no (J. Ma).

https://doi.org/10.1016/j.cirpj.2023.12.007
Received 4 October 2023; Received in revised form 29 November 2023; Accepted 12 December 2023
Available online 28 December 2023

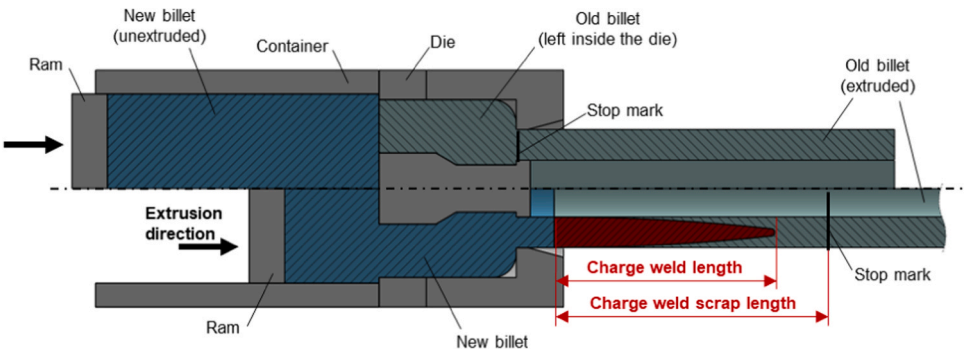

Fig. 1. Evolution of charge weld in a porthole die.

the sheared face often contains lubricant and oxidized metal from the shear blade, which can lead to a discontinuity in the extruded profile [5] leading to the charge weld zone with substandard mechanical properties and integrity. In industrial practice, therefore, the regions of the extruded profile showing traces of charge welds are normally considered in-process scrap.

During the past two decades, there has been a growing number of studies focusing on charge weld mechanisms. To name a few, Valberg [34] conducted a comprehensive review of extrusion welds in aluminum extrusion, providing up-to-date information until 1998. Some researchers, such as Loukus et al. [14], Den Bakker et al. [5], Lou et al. [13], Yu et al. [37], and Tang et al. [32], conducted experimental studies to investigate the evolution of the mechanical properties within the charge weld zone. They specifically studied how the properties relate to the transition zones from old to new billets. Additionally, Nanninga et al. [18,17] explored the impact of charge weld on the fatigue life of extruded profiles. A recent work by Oberhausen and Cooper [21] proposed an analytical model for the prediction of the strength of the material in the charge weld. Their model builds upon the film theory of solid-state welding and incorporates the plane-strain welding model developed by Cooper and Allwood [4]. While the model successfully captures some observed experimental trends, its predictive accuracy still requires further refinement. Overall, all these studies consistently indicate that the charge weld zone exhibits lower mechanical properties compared to the extruded parent material unaffected by the transition between two successive billets.

Experimental studies of charge weld evolution require extensive work, which is time-consuming and expensive. To effectively predict the scrap length cut away due to charge weld, two analytical models were proposed by Saha [25] and Jowett et al. [10]. Despite the fact that analytical models can offer estimates of the scrap length, recent studies conducted by Reggiani and Donati [27], Reggiani et al. [28], and Negozio et al. [20,19] suggest that these analytical formulations normally provide a strong underestimation of the charge weld scrap length.

To more accurately analyse the charge weld behaviour, numerical investigations have been conducted for the prediction and reduction of charge weld length by optimizing extrusion parameters and die design. In solid profile extrusion, several pioneering works were conducted by Li et al. [12], Hatzenbichler and Buchmayr [9], and Mahmoodkhani et al. [15,16]. Two-dimensional and axisymmetric finite element (FE) models using the updated Lagrangian method were established to analyse charge weld evolution in rod extrusion. Li et al. [12] found that the charge weld length strongly depends on the rate at which the material in the dead metal zones flows out. It was suggested that the roundness of the die corners facilitates local metal flow, which can lead to faster removal of the material in the dead metal zone, thereby shortening the charge weld scrap length. Similarly, Mahmoodkhani et al. [15,16] found that a tapered feeder design decreases the size of the dead metal zone compared to a flat feeder, leading to easier removal of the old materials from the die and thus a shorter charge weld zone. Hatzenbichler and Buchmayr [9] also found that a decrease in the height and diameter of the feeder chamber reduces the length of the charge weld. However, the underlying reasons for this effect remain unclear. On the other hand, Pinter et al. [23], Yu et al. [36] and Truong et al. [33] developed three-dimensional FE models using the Arbitrary Lagrangian-Eulerian scheme to gain new insights into charge weld evolution under varying die design parameters. The study on web (bridge) shape, Yu et al. [36], indicates that the effect of the welding chamber height is negligible. It is also reported that square webs conclude with longer charge weld than pointed webs but with no clear explanation. Truong et al. [33] studied how charge weld is affected by two different die designs, including pocket and spreader dies. They found that the charge weld length for the pocket die was about half that of the spread die due to the smaller volume within the pocket die.

Considering hollow profile extrusion, however, there is a limited body of research available studying the relationship between extrusion parameters and charge weld properties. Pinter et al. [23] found that a die design with two webs can lead to longer charge weld than those with three and four webs, primarily due to extended dead metal zones and increased port volume. Chen et al. [3] conducted a comparative numerical study using a pyramid die and a conventional porthole die, showing that a larger pyramid angle increases the stock of old billet in the die, which retards the onset of charge weld. However, this is limited to a numerical study only, indicating that further experimental validation is needed. A study on the effect of porthole volume and shape by Pinter et al. [24] showed that conical ports result in increased pressure in the porthole, permitting the reduction of the dead metal zone and thus shortening the charge weld length. It is also reported that the billet temperature and ram speed have a negligible effect on charge weld length, yet without providing a clear explanation. Zhang et al. [39] conducted an in-depth examination of the die design effect in terms of the height of the baffle plate, the corner radius of the welding chamber and the sinking depth of the die web. Their work reported that the distribution of material flow velocity through the profile's cross section can be homogeneous with an increase in the height of the welding chamber, this tends to reduce charge weld length. Additionally, increasing both the sinking depth of the die web and the corner radius of the welding chamber allows the old material left in the die to flow out more easily, shortening the charge weld length.

Despite the research reported in the literature, the behaviours and mechanisms of charge weld evolution in hollow profile extrusion are not well understood. This limits the effective control of the extrusion process from both economical and sustainable manufacturing perspectives. To gain further insights into this phenomenon, therefore, the present study focuses on investigating the evolution of charge weld in AA6060 circular tube extrusion by combining full-scale industrial experiments done under real-world conditions and advanced numerical modeling approaches. The purpose is to seek answers to the following two research questions:

RQ1. : What are the underlying mechanisms of charge weld formation

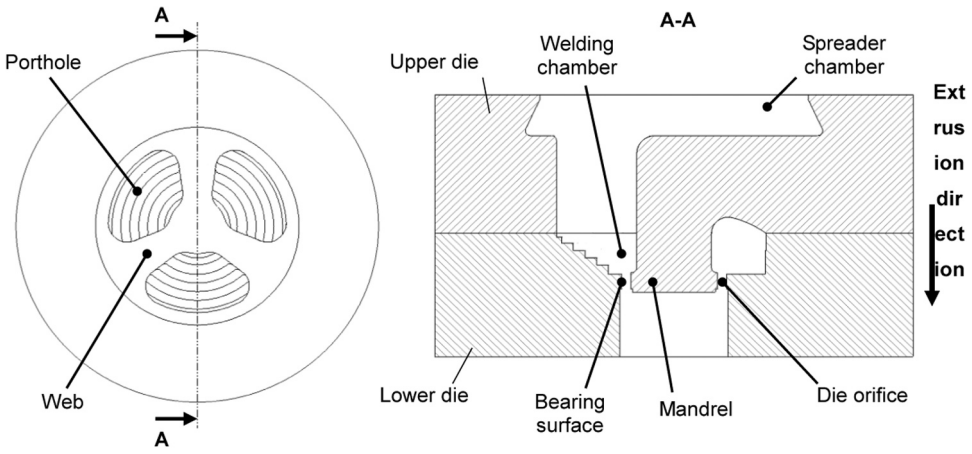

Fig. 2. Extrusion die geometry used in the experiments.

Table 1
Process parameters and tooling geometries.

Billet diameter	203	mm
Billet length	750	mm
Billet temperature	460	°C
Temperature taper	40	°C
Ram speed	11.5	mm/s
Extrusion ratio	33	/
Butt-end length	30	mm
Container temperature	420	°C
Container diameter	210	mm
Die temperature	450	°C

Note: Shared temperatures correspond to the initial values.

and evolution along extruded profiles, and how can these be accurately predicted using industrial experiments and numerical modeling?

RQ2. : How do changes in the characteristics of charge weld correlate with the material flow mechanism and the dead metal zone when subjected to different process parameters?

The remainder of this paper is organized as follows: Firstly, a series of carefully controlled industrial extrusion experiments to examine the occurrence of charge weld zones between two successive billets is presented. Characterization experiments were conducted to identify the formation and evolution of the charge weld and assess its extension along the extruded tube. The next part presents a numerical model based on the QForm 10.2.1 software developed to predict the charge weld evolution and scrap length. Based on the experimental findings, a comparison between the charge weld prediction of the numerical model along with two analytical models available in the literature, is presented. Subsequently, a numerical sensitivity study for charge weld behaviours is presented, exploring the effect of ram speed and billet temperature on the evolution characteristics of charge weld, with a particular focus on material flow and dead metal zone. Finally, the conclusions and outlook of this paper are presented.

2. Experiments and modeling

2.1. Extrusion experiments of aluminum circular tube

Industrial experiments were conducted on a 22 MN extrusion press at Benteler Automotive Raufoss AS (Raufoss, Norway). AA6060 circular tube is used as a basis for this research. Fig. 2 shows the cross-sectional view of the single-cavity porthole die. The die comprises a spreader chamber and three portholes positioned symmetrically around the perimeter, aiming for a balanced material flow through the welding

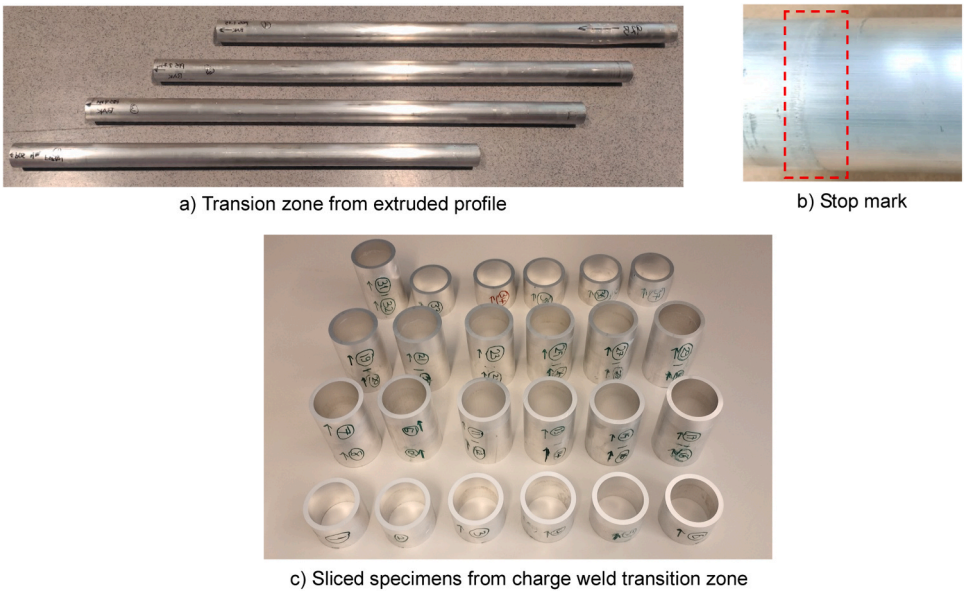

Fig. 3. Sample preparation after the extrusion process.

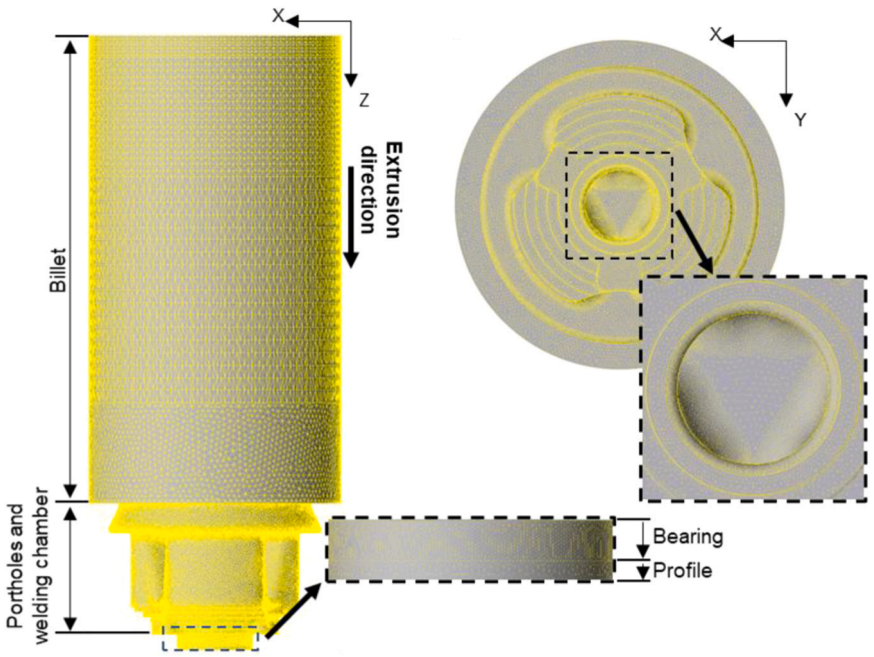

Fig. 4. Numerical modeling.

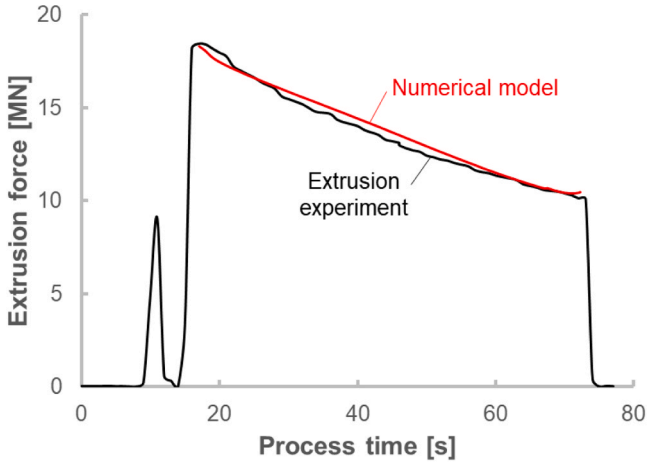

Fig. 5. Comparison of extrusion load between extrusion experiment and numerical model. The initial stages of extrusion process, including upsetting and die-filling, are highlighted in the experimental results.

chamber. The bearing length remains fixed at 9 mm around the perimeter of the die outlet. The circular tube has a uniform nominal thickness of 5.5 mm, with a cross-sectional area of 1000 mm^2.

60 billets of AA6060 were consecutively extruded in each batch using the process parameters listed in Table 1. It should be noted that the initial temperatures represented in the table were selected based on Sheppard [31] and Saha [29]. Furthermore, a temperature taper was applied to the billet, resulting in a lower initial temperature at the rear of the billet to better resemble isothermal extrusion, hence compensating for the mechanical heat generated during extrusion. The extruded profile temperature was measured using a digital infrared thermometer; however, challenges in accurate in-situ measurements were encountered due to light reflection deviations caused by the circular shape. Consequently, deviations between the measured temperature and the actual temperature of the extruded circular tube were noted. In the experiments, the extrusion load was continuously recorded throughout the process (Fig. 5). To examine the evolution of charge weld under 'steady-state' operational conditions, particular attention was given to investigating the transition zone of the profile between the 10^{th} and 11^{th} billets. Directly after extrusion, a cooling procedure involving both air and water was employed to quench the profile.

2.2. Experimental characterization of charge welds

To investigate the charge weld evolution, a transition segment with a length of 4000 mm from the stop mark was collected (Fig. 3a). Fig. 3b shows the stop mark caused by the profile sticking to the bearing surface upon stopping the ram. Here, the stop mark serves as a reference point to describe the location of the charge weld.

The collected profile length was then sliced into segments with an interval of 100 mm. Additionally, the sliced samples from the onset and end of the charge weld zone were further sliced at a distance of 50 mm, allowing for a more detailed investigation of the charge weld evolution in those zones of the extruded profile (Fig. 3c).

To make the macrostructure of the charge weld visible for analysis, the sliced samples were subjected to a series of preparation steps, including grinding with abrasive papers, polishing and subsequent etching. The solution mixture used for etching comprised a sodium hydroxide solution of 30% concentration in a litre of distilled water. The solution was heated to 60 °C and etching was conducted for a duration between 60 and 90 s. Afterwards, the charge weld became visible even to the unaided eye. However, for in-depth analysis, digital images of each sample surface were captured using digital photography. To identify the charge weld pattern, open-source image analysis software, ImageJ, was used to calculate the percentage area of the new billet in the cross-section of each sample until reaching the selected limit of 99.5%. In the extrusion industry, the conventional consideration is that the threshold value for the charge weld to vanish corresponds to the sample when the section consisted of, say, 95% material from the new billet. This is because of the challenges associated with evaluating the material behaviour when the new billet material approaches the profile surface. However, here, following the report by Negozio et al. [20], it was assumed that the corresponding threshold is 99.5%.

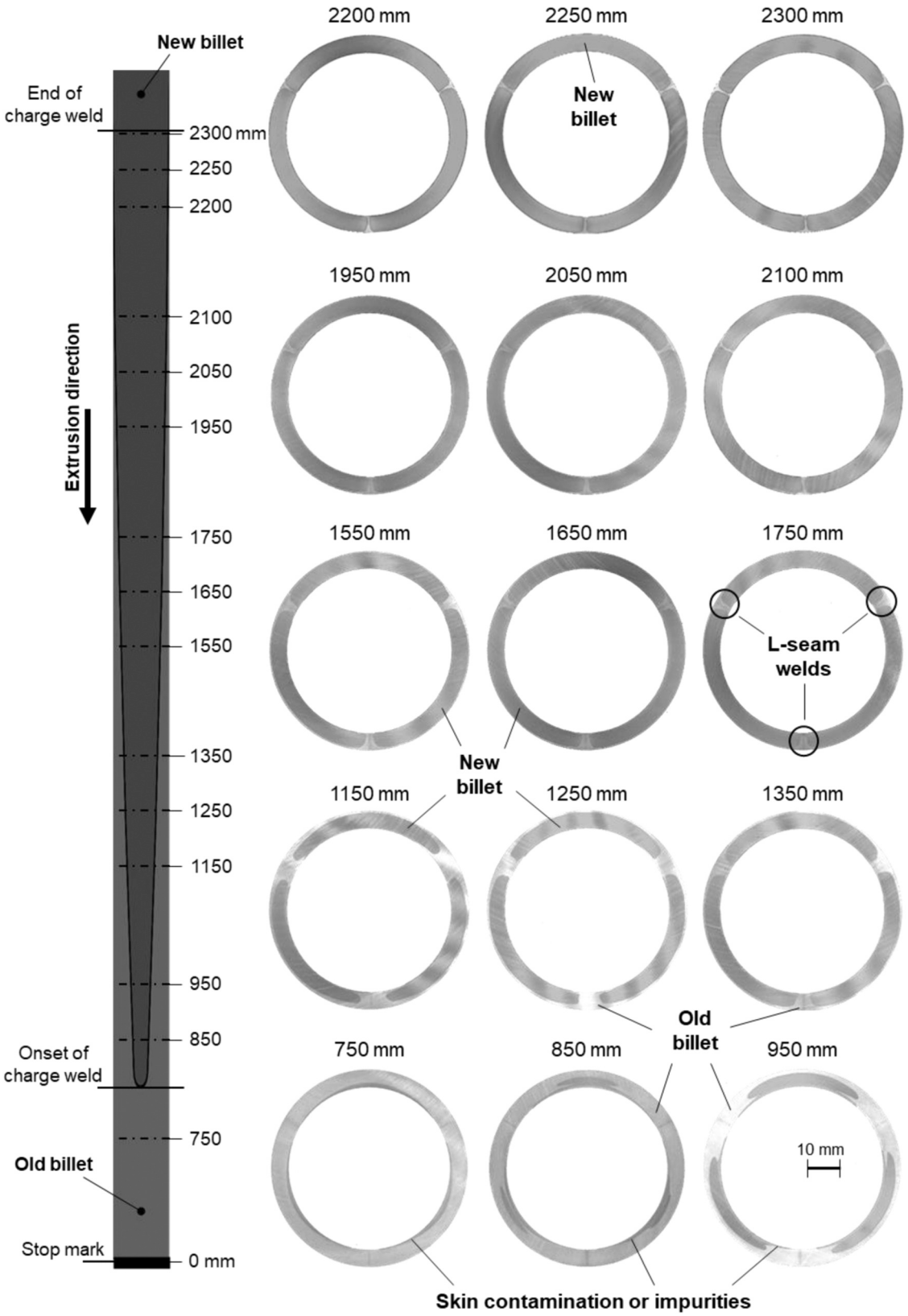

Fig. 6. Evolution of charge weld between two successive aluminum billets.

2.3. Numerical modeling

A finite element model of the extrusion process was developed based on QForm-Extrusion 10.2.1 [26], aiming to provide a more detailed examination of the charge weld evolution mechanisms in the extruded profiles. QForm-Extrusion is a commercially available FE package that employs the Arbitrary Lagrangian-Eulerian (ALE) approach, specifically optimized for extrusion processes [7]. Charge weld phenomena analysis

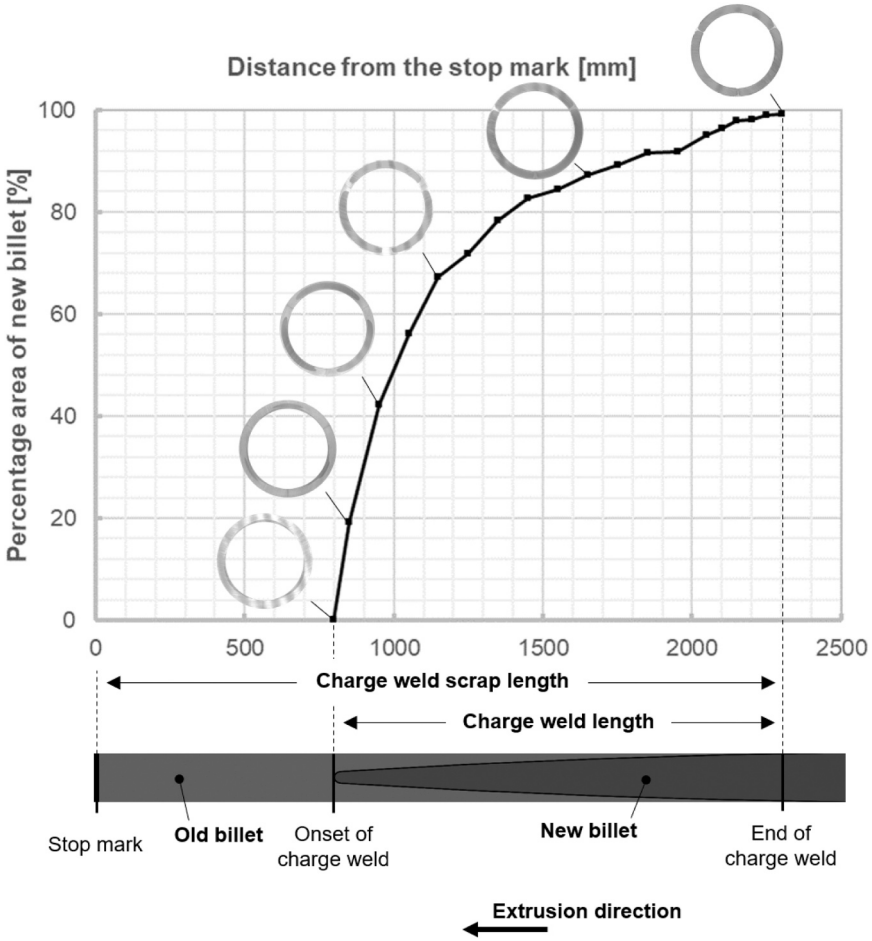

Fig. 7. Charge weld evolution observed in experimental analysis.

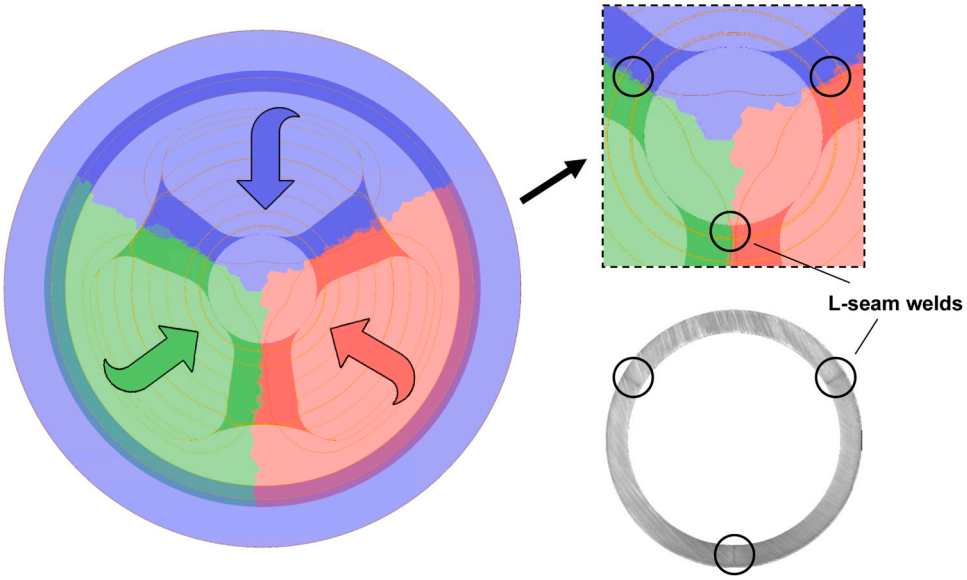

Fig. 8. Position of longitudinal seam welds in both experimental and numerical analyses.

was assumed to not require coupled analysis between material flow and deformation of tools and support conditions. The full (complete) numerical model was also considered essential because symmetry boundary conditions could significantly influence the charge weld evolution mechanism. Consequently, the main components of the model were divided into four groups: billet, porthole and welding chamber, bearing, and profile (Fig. 4). The extrusion tools were modelled as rigid, and the only deformable body was the billet. Moreover, QShape, an integrated program capability of QForm that enables volumetric mesh generation of process components, was used to perform the discretization of the

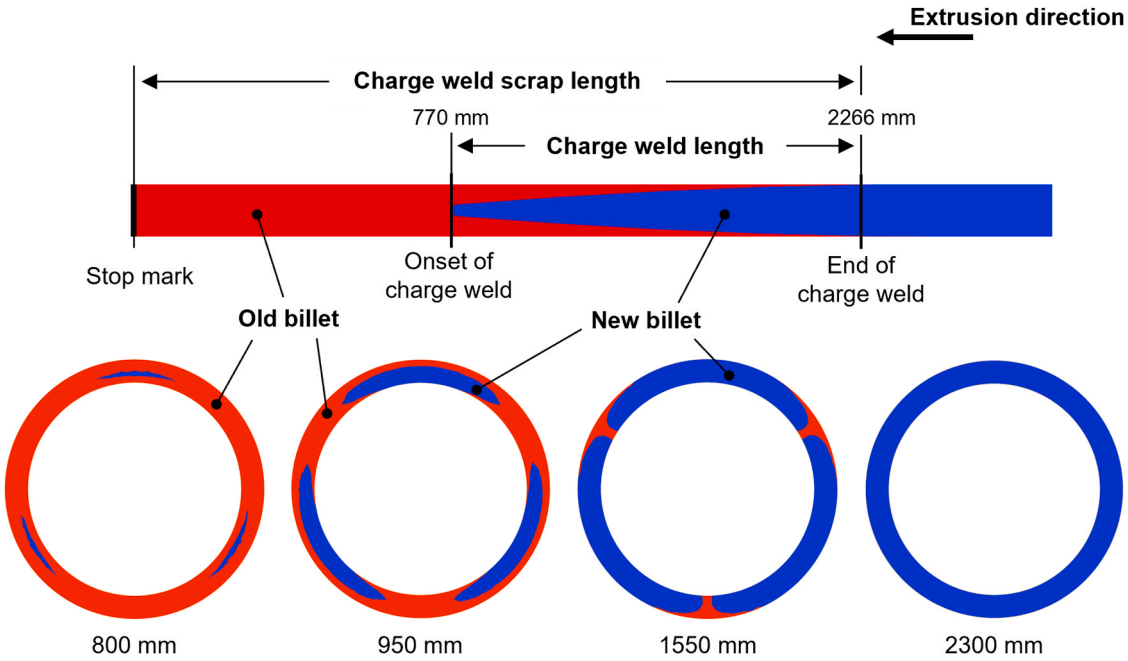

Fig. 9. Numerical analysis of charge weld evolution. The distance from the stop mark is indicated under each figure.

extrusion tools and billet, using 3D tetrahedral 4-noded elements. To accurately capture the material behaviour in areas with high-strain (rate) gradients, the elements were significantly refined in the bearing region, as shown in the figure.

The material flow stress-strain rate-temperature behaviour of the commercial AA6060 alloy used was modelled with an isotropic-viscoplastic model, using the Sellars-Tegart inverse sine hyperbolic function [30], also called the Zener-Hollomon model [38], given as follows:

$$\overline{\sigma} = \frac{1}{\alpha}\sinh^{-1}\left[\left(\frac{Z}{A}\right)^{\frac{1}{n}}\right] = \frac{1}{\alpha}\sinh^{-1}\left[\left(\frac{\dot{\varepsilon}\exp(Q/RT)}{A}\right)^{\frac{1}{n}}\right] \quad (1)$$

where $\overline{\sigma}$ is flow stress, and α, n and A are temperature-independent material constants, Q is the activation energy, R is the universal gas constant, and T is the absolute temperature. The values used in the simulation were adopted from the hot torsion test conducted by Verlinden et al. [35], with Q= 161 kJ/mol, R= 8.314 J/(K mol), $\alpha = 0.035$ 1/MPa, $n = 4.67$, A= 0.76301E11 1/s and T is expressed in Kelvin.

The so-called Levanov friction coefficient — a generalized form of the Coulomb and Siebel friction laws — was adapted to the model using the following formula [11]:

$$\tau_L = m\frac{\overline{\sigma}}{\sqrt{3}}\left[1-\exp\left(-L_n\frac{\sigma_n}{\overline{\sigma}}\right)\right] \quad (2)$$

In this equation, τ_L is the friction stress, m ($0 \le m \le 1$) is the friction constant, σ_n is the normal stress, $\overline{\sigma}$ is the equivalent flow stress and L_n is the Levanov coefficient. When the normal contact pressure between the deforming material and the tool is low, such as in the outer part of the bearing region, the frictional stresses closely resemble those in Coulomb's model. Conversely, when the normal contact pressure is high, such as when it takes less energy to deform the material than sliding against the die surface, typically at the container-billet interface (m=1 full sticking condition), the shear stresses closely resemble those in Siebel's model. Based on Bandini et al. [1], the Levanov coefficient in the aluminum extrusion was set to 1.25, and the heat transfer coefficient between the billet and the tool was set to 11000 W/m^{2}K. In addition, the heat transfer coefficient between billet-air and tooling-air interfaces was set to 30 W/m^{2}K, while the air temperature was considered as fixed at 20 °C.

During the calculation of charge weld formation, the assumption was made that the butt-end underwent removal through shearing prior to each extrusion process, while the extrusion die remained filled with material, as illustrated in Fig. 1. The charge weld formation was computed using a transient analysis approach with moving boundaries implemented in QForm-Extrusion. In this particular problem, the time-dependent boundary conditions for the flow and heat transfer equations are considered. Initially, the Lagrange model is employed, allowing the adaptation of the finite element mesh to follow the material flow and precisely track the die-filling progress. Once the die-filling stage is completed, and the material reaches the die orifice, the simulation transitions to the ALE model, assuming that the tool is already filled [2]. This approach significantly reduces the number of elements and remeshing attempts. Specifically, the mesh in the profile, porthole, welding chamber, and bearing remain fixed, while in the billet region, the size of elements scales down linearly in the extrusion direction at each time step. The computational time for the model was 14 h on a 112-core Xeon processor using parallel processing, and 256 GB of RAM.

The initial validation involved a comparison between the experimentally measured and numerically predicted extrusion loads. The maximum experimental extrusion force is 18.4 MN, while the predicted force is 18.3 MN. As shown in Fig. 5, the model captures remarkably well the maximum extrusion force behaviours with only a slight difference of less than 1%, and the minimum extrusion force with a difference of just around 3%. Consequently, from the view of extrusion load, the accuracy of the established FE model is considered accurate and acceptable for the purpose of this study. In the following, therefore, the force-based validated model will subsequently be used to verify the prediction of charge weld evolution and to gain additional insight into the charge weld mechanism in hollow aluminum profiles.

3. Results and discussion

3.1. Charge weld evolution

Following the etching processes, digital images of the sample's surfaces were captured to trace the charge weld evolution resulting in the transition zone between two successive aluminum billets. Fig. 6 shows

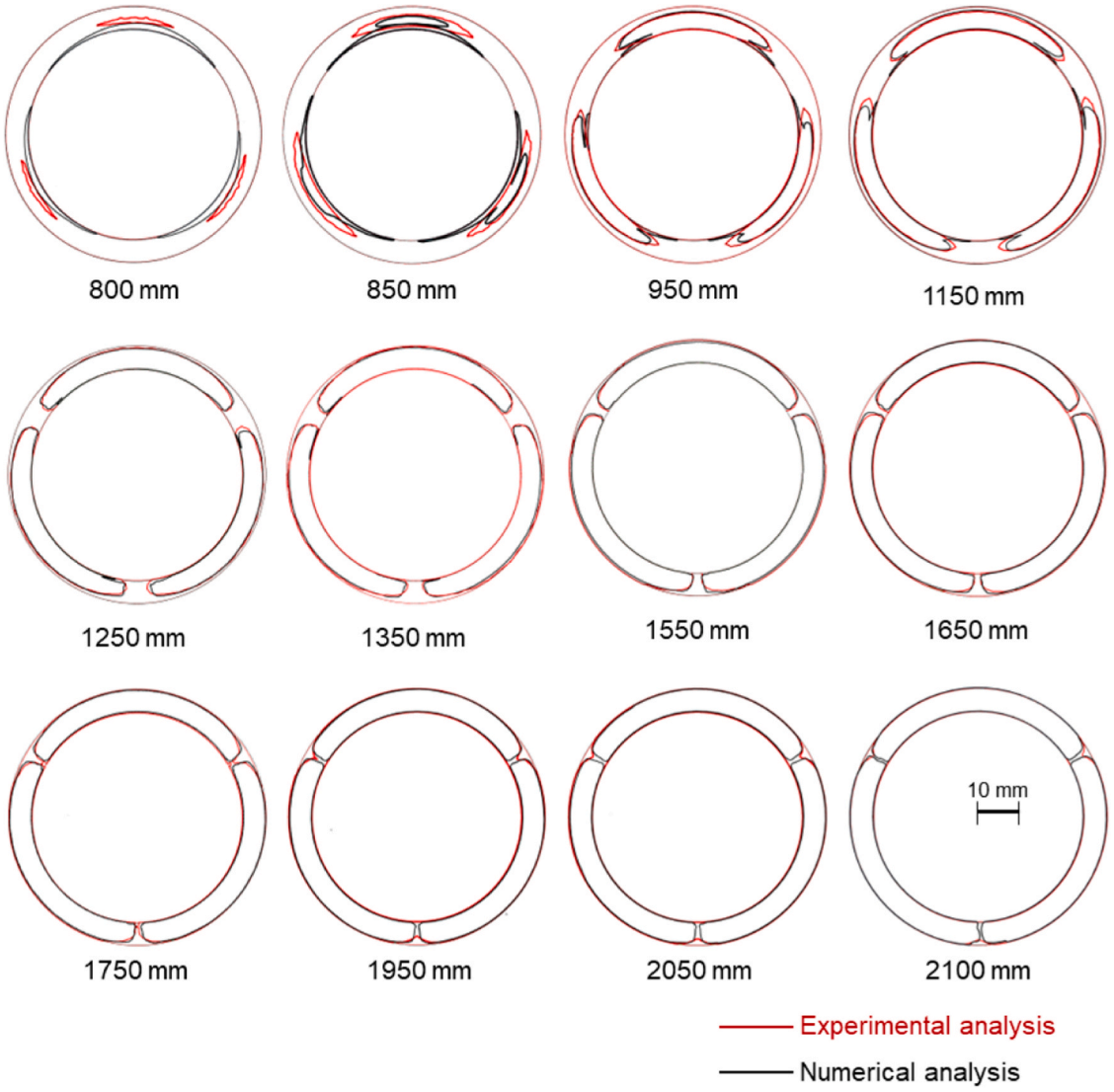

Fig. 10. Comparison of charge weld evolution between cross sections obtained from the experimental and numerical analyses. The distance from the stop mark is indicated under each figure.

the charge weld pattern observed in the extruded profile between the 10^{th} and 11^{th} billets. These patterns reveal that the charge weld appears in the form of three identical 'tongues' in the cross-section, each extending across one-third of the profile's cross section. Moreover, these tongues are positioned on both sides of the longitudinal seam welds (L-seam welds). This alignment is a consequence of the charge weld being in line with the contour of the identical metal streams, which are divided by the die webs and feed the profile through equally distributed portholes (as shown in Fig. 8).

As shown in Fig. 6, a defect is observed near the inner surface of the profile, just at the onset of the charge weld zone. The study conducted by Negozio et al. [19] focusing on skin contamination defects reveals that as the charge weld interface approaches the skin contamination, defects become narrower and shift to one side, eventually leading to complete section replacement accompanied by the charge weld. Therefore, it appears that at the onset of the charge weld zone, a replacement occurs between the charge weld and the potential of skin contamination or other impurities within the old billet left inside the die. Moreover, the figure shows that the charge weld arises in the middle of the thickness at a distance between 750 mm and 850 mm from the stop mark (see first and second cross section in the figure). As a result, the onset of the charge weld could be considered to occur at a location, say, 800 mm from the stop mark. Subsequently, migration is observed towards both the inner and outer surfaces. These two behaviours could be attributed to the material flow difference in the extrusion die, with faster flow in the middle of the portholes and slower flow near the billet-die interfaces. Moreover, the figure indicates that the transition zone ends 2300 mm away from the stop mark.

To quantitatively assess the evolution of the charge weld, the percentage area of the new billet was calculated as a function of distance from the stop mark, as shown in Fig. 7. The figure shows that the material replacement of the old billet by the new billet is fast in the beginning, then gradually decreases towards the end of the transition zone.

3.2. Prediction and analysis of sectional distribution of charge weld

An investigation was conducted to numerically predict and analyze the charge weld evolution during the transition between two successive aluminum billets. First, the L-seam weld positioning was analysed to better understand the evolution of the charge weld in the profile's cross section. The material is separated into multiple streams by the die webs and rejoined in the welding chamber, forming the L-seam welds along the entire profile length. As a result of employing three equal portholes

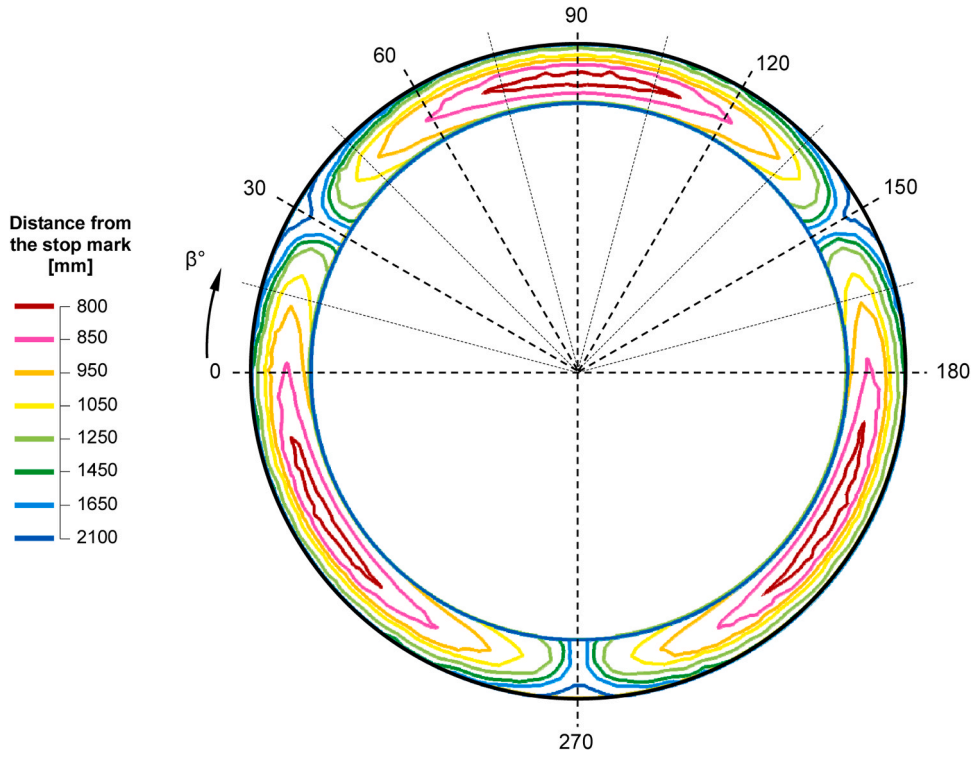

Fig. 11. Collective investigation of charge weld evolution across the profile's cross section. Cross-sectional data was acquired at various distances from the stop mark.

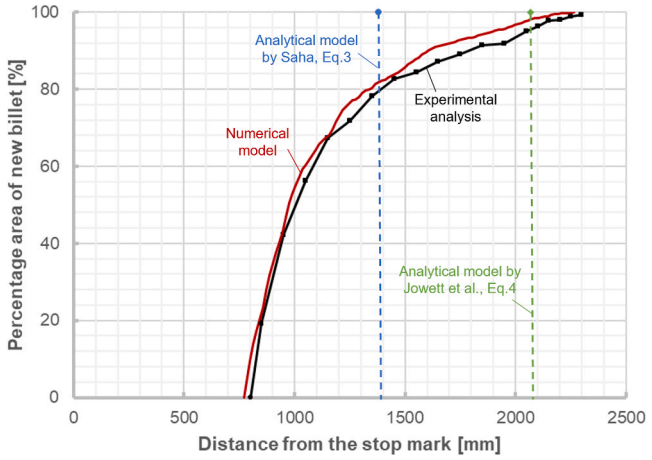

Fig. 12. Prediction of charge weld by numerical model and analytical models.

Table 2
Process parameters used in numerical analyses.

Process parameters	Values
Ram speed [mm/s]	3, 6, **11.5**, 24
Billet temperature [°C]	430, **460**, 490

Note: Parameters used in extrusion experiments are indicated in bold.

in the die design, it is expected that L-seam welds will be uniformly distributed around the profile, following the symmetry axis of the die web. Fig. 8 illustrates the rejoining of material streams within the welding chamber, leading to the formation of L-seam welds that are evenly distributed around the profile at 120° intervals. These findings were further validated through the analysis of experimental samples, specifically at a distance of 2500 mm from the stop mark.

Second, the numerical investigation focused on the charge weld formation. The numerical findings concerning the replacement of the old billet with the new billet at various distances from the stop mark are presented in Fig. 9. The onset of the charge weld was predicted to occur at 770 mm from the stop mark, while the end of the charge weld was predicted to be located at 2266 mm from the stop mark. Subsequently, to validate the numerical findings, a comparison was made between the cross sections collected from the experimental and numerical analyses. For this purpose, the percentage of new billet on each profile's cross section was calculated. A comparison of charge weld evolution in the profile's cross sections collected at different distances from the stop mark is shown in Fig. 10. The model accurately captures the evolution of the charge weld with errors ranging from 1.5% to 7.5%, except for the initial stage of the charge weld. This discrepancy could be attributed to the potential presence of skin contamination or impurities in the charge weld zone, as discussed in the previous section. Furthermore, another discrepancy was observed as the charge weld approaches the L-seam welds. This could be due to the interaction of charge weld and L-seam welds since the numerical model is unable to simultaneously depict the evolution and interaction of charge weld and L-seam welds, potentially resulting in the observed difference.

A numerical examination of charge weld formation was conducted for the profile's cross-sections in the transition zone between two consecutive aluminum billets, following the methodology proposed by Duplancic and Prgin [8]. Fig. 11 was generated by compiling cross-sectional data obtained at various distances from the stop mark, enabling the examination of charge weld evolution. It can be found that the charge weld occurs in the middle of the thickness. The figure also highlights a more pronounced accumulation along the inner and outer walls, as well as around the L-seam welds located at $\beta = 30°$, 150° and 270°, as shown in Fig. 8. There is a noticeable difference between the peripheral areas and the central region of the section, with the peripheral areas exhibiting a lag in terms of line accumulation. This difference

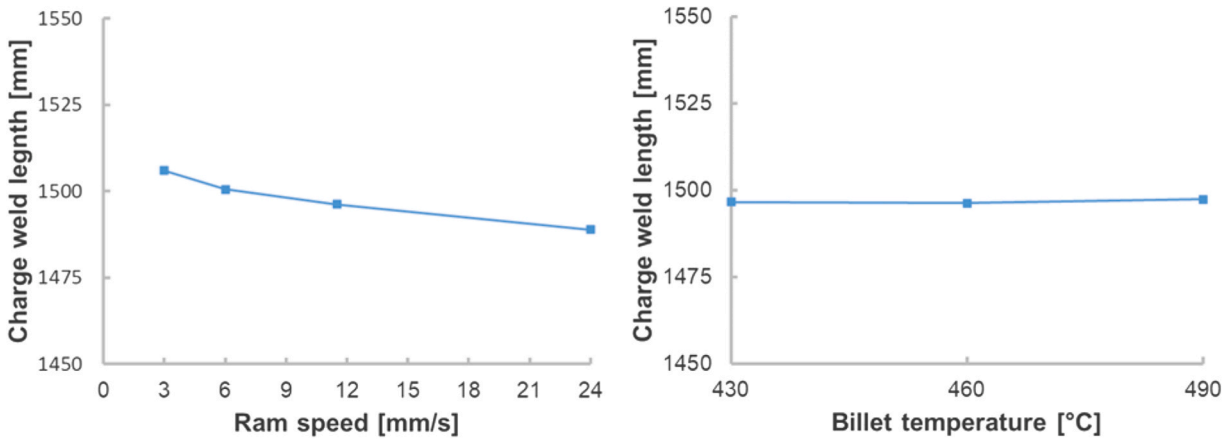

Fig. 13. Sensitivity of charge weld length to ram speed and billet temperature.

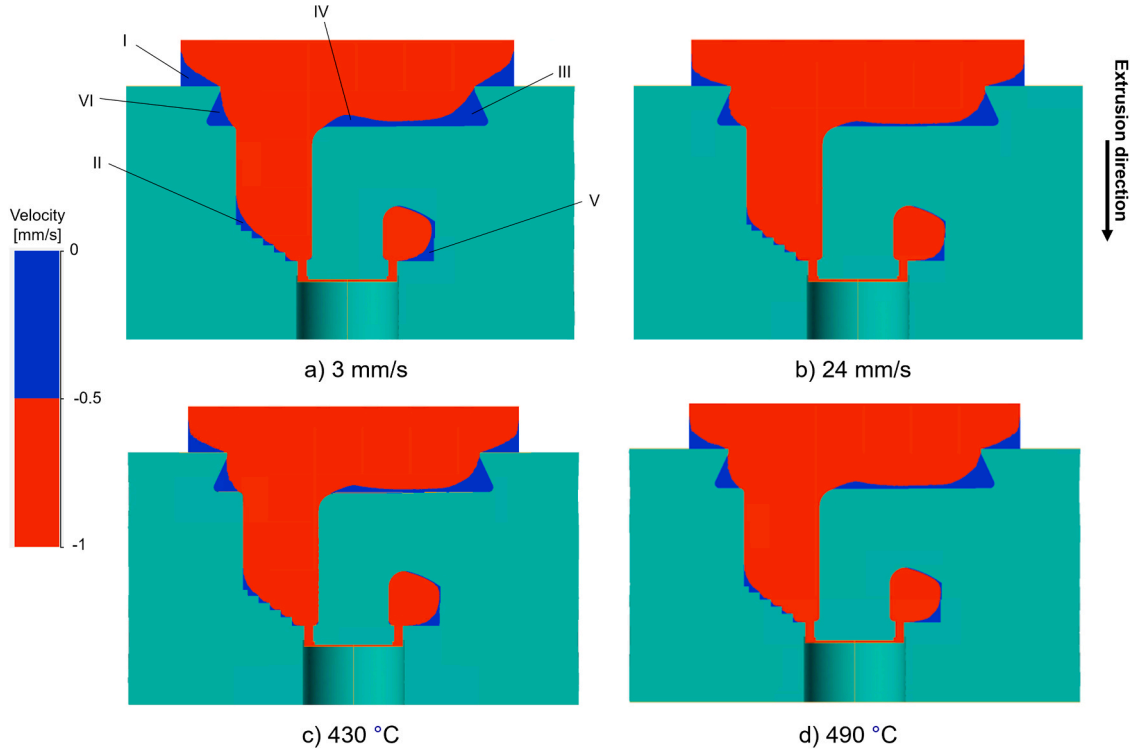

Fig. 14. Velocity distribution on die cross section for minimum and maximum (a-b) ram speeds and (c-d) billet temperatures.

arises due to the discrepancy in material flow within the extrusion die. The central region of the portholes and bearing experiences faster flow, while the peripheral areas have slower flow due to friction between the die and billet interfaces.

3.3. Prediction and analysis of charge weld scrap length

The charge weld length and the associated charge weld scrap length were analyzed using the developed numerical model. For comparison, the charge weld scrap length was also calculated using the two analytical models provided in the literature, as given in Eqn 3 and 4 below. Fig. 12 shows the numerical and experimental findings of the new billet's percentage occurrence in the profile cross section as a function of distance from the stop mark. The onset of charge weld was predicted numerically to occur at 770 mm from the stop mark and end at 2266 mm. These predictions closely align with the experimental findings, where the onset of charge weld was found to occur at 800 mm away from the stop mark, and the end was observed at 2300 mm. Notably, the numerical model demonstrates high accuracy in predicting the end of the charge weld, with an error of less than 1.5%, while the onset of the charge weld shows an error of just over 3.7%. Furthermore, the numerical model accurately captures the evolution of the charge weld in terms of new billet percentage on the profile's cross section, displaying a difference of only 7.5% from the experimental findings, and following the same trend.

For comparison, the charge weld scrap length was estimated by using two representative analytical models offered in the literature. The first model, developed by Saha [25], is represented as follows:

$$d = \frac{(V_1 + V_2)}{A_E\, n} \tag{3}$$

where d represents the charge weld scrap length, while V_1 and V_2 are the total volume of metal left in the die portholes and weld chamber from

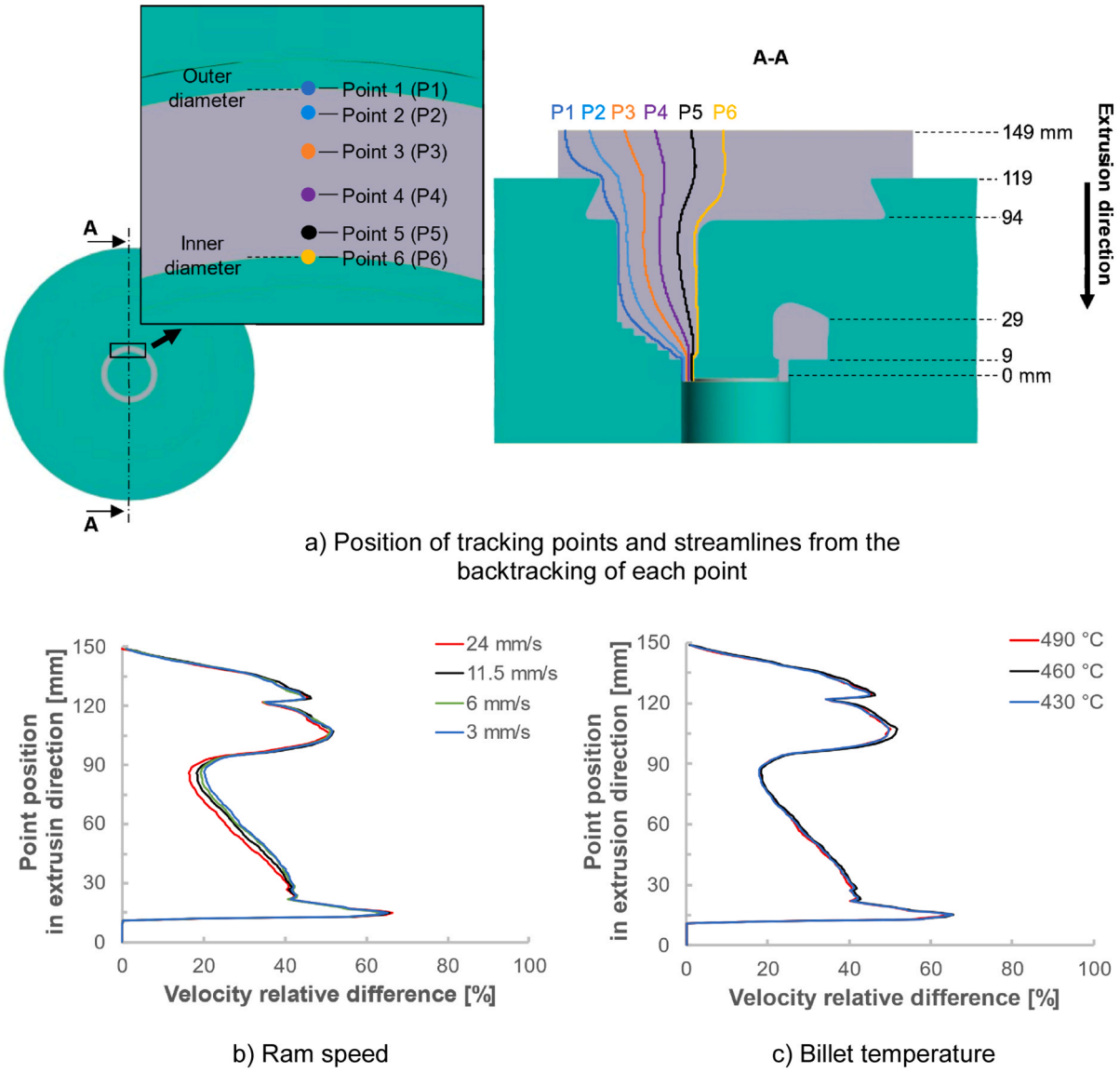

Fig. 15. Material flow analysis within the extrusion die.

the old billet, respectively. A_E is the cross-sectional area of the extruded profile and n is the number of die openings.

A second model, proposed by Jowett et al. [10], takes into account the presence of dead metal zones and slower material flow in the peripheral zone of the portholes, introducing a corrective factor of 1.5, expressed as follows:

$$d = 1.5\ \frac{(V_1 + V_2)}{A_E\ n} \tag{4}$$

As shown in Fig. 12, the charge weld scrap length was estimated at 1379 mm and 2069 mm by Eqs. 3 and 4, respectively. This is much lower than the experimental result (charge weld scrap length of 2300 mm). More importantly, the two analytical models underestimate the charge weld scrap length, with prediction errors of just over 40% and 10%, respectively. Despite the inclusion of a correction factor in Eqn 4, the observed discrepancy between the analytical models considered and the experimental result could be attributed to the presence of dead metal zones and the discrepancy of the material flow between the centre of portholes and their peripheral zones, as well as between the bearing and its peripheral zone.

3.4. Effects of process parameters on charge weld length and evolution of sectional distribution

Upon noting a disparity between experimental findings and analytical calculations, potentially attributed to the absence of correction factors, there arises a necessity to explore the correlation between process parameters and charge weld evolution. Based on the validated FE model, a set of numerical analyses was performed by varying ram speeds and billet temperatures. The investigated ram speeds and billet temperatures are shown in Table 2, guided by values reported in related literature, specifically Sheppard [31] and Saha [29]. In addition, two main aspects of the process parameters, i.e., ram speed and billet temperature were examined to determine their effects on material flow and dead metal zones during the extrusion process.

First, the sensitivity of charge weld length to ram speed and billet temperature was investigated, as shown in Fig. 13. The figure shows that the charge weld length is slightly affected by the ram speed, in which increased speeds lead to shorter charge weld lengths. However, no significant change was observed for different billet temperatures.

To comprehend the underlying mechanism behind the findings of sensitivity analyses, the velocity distribution within the extrusion die

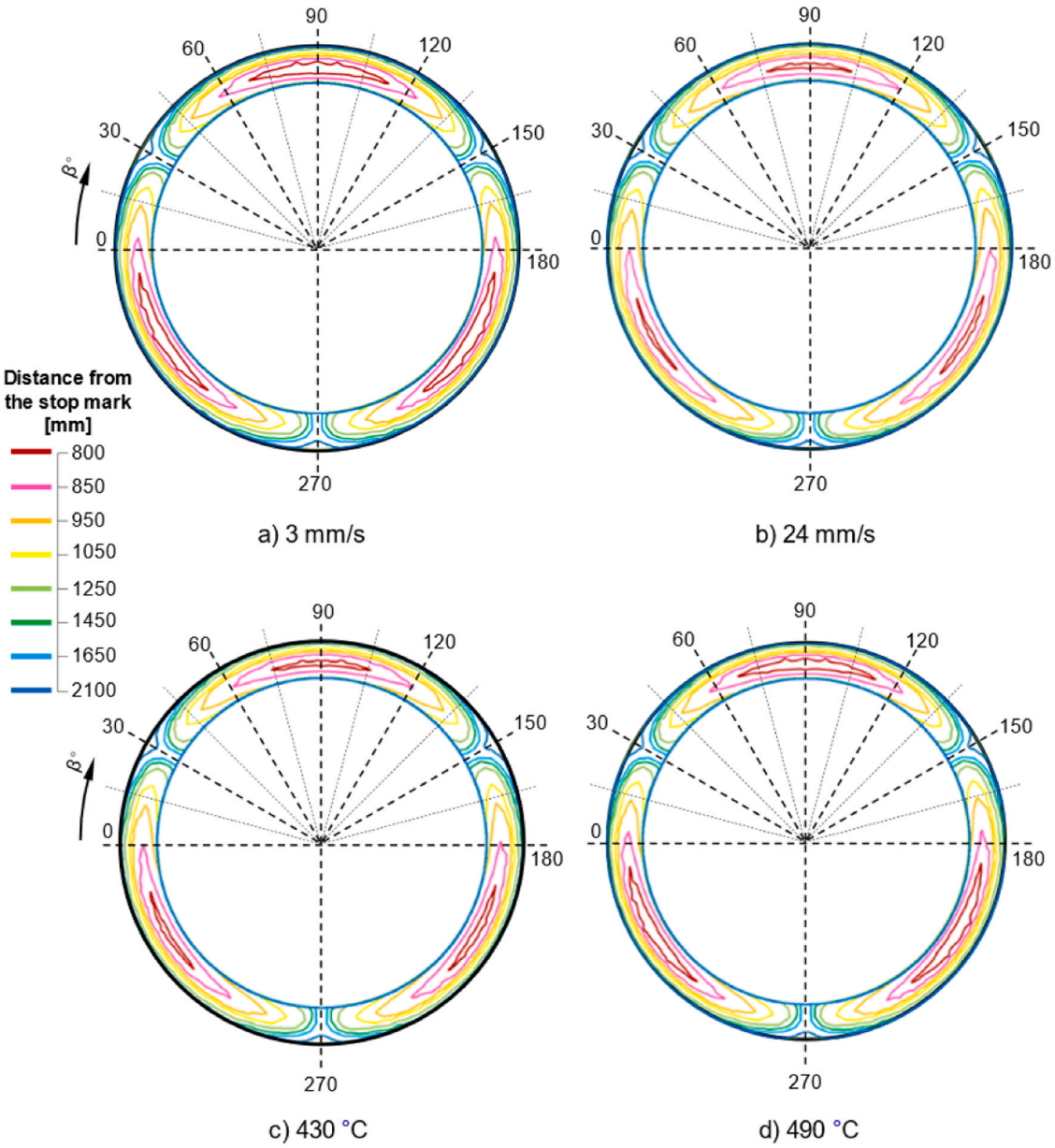

Fig. 16. Cross-sectional investigation of charge weld evolution for minimum and maximum (a-b) ram speeds and (c-d) billet temperatures. Cross-sectional data was acquired at various distances from the stop mark.

was evaluated for minimum and maximum ram speeds and billet temperatures, as shown in Fig. 14. The figure shows the presence of the dead metal zone formed at various locations as a result of complete extrusion push, as previously observed by Valberg [34]: (I) in the peripheral flat face of the die, (II) in the welding chamber, (III) in front of the webs, (IV) in front of the flat front face of the mandrel, (V) in the welding chamber at the rear end of the webs, and (VI) in the spreader chamber. The figure indicates that the dead metal zone in the corners increases with decreased ram speed, while billet temperature has a negligible effect on the dead metal zone. This may be explained by the friction between the billet material and the surface of the dead metal zone. Saha [29] reported that the generated dead metal zones behave like a conical die surface as the material continues to extrude, leading to a deceleration in material flow around the dead metal zones. Consequently, the dead metal zone was found to be smaller for the higher velocities, resulting in a relatively shorter charge weld length. Conversely, the dead metal zones appeared similar for different billet temperatures, leading to no significant change in the charge weld length. This observation is in line with the findings by Pinter et al. [24].

To further study the material flow, an examination was conducted of the evolution of velocities along the extrusion die under different ram speeds and billet temperatures by backtracking six points on the profile front face. The position of tracking points and streamlines resulting from the backtracking of each point are depicted in Fig. 15a. A formulation known as velocity relative difference (VRD) was introduced by Zhao et al. [40] to assess the degree of uniformity in the velocity distribution across the cross section of the extruded profile. Here, the formulation has been adapted to describe the degree of flow balance within the die, as follows:

$$VRD = \frac{\sum_{i=1}^{n} \frac{|v_i - v_a|}{v_a}}{n_p} \times 100\% \tag{5}$$

where v_i is the velocity at point i along the streamlines, v_a is the average velocity of all points at the same position in the extrusion direction, and n_p is the number of the points tracked. As reported by Zhao et al. [40], a

smaller VRD indicates a more homogeneous material flow through the die. Fig. 15b and Fig. 15c present plots of VRD for different ram speeds and billet temperatures. It is noticed from Fig. 15b that the material flow becomes more homogenous within the portholes of the die as the ram speed increases, resulting in a relatively shorter charge weld length. However, Fig. 15c indicates no difference in material homogeneity for varying billet temperatures, and as a result, no significant change in the charge weld length is found.

Finally, the charge weld formation history of the profile's cross sections in the charge weld zone was investigated for minimum and maximum ram speeds and billet temperatures, using the previously described method. Fig. 16 shows the collective examination of charge weld evolution on the profile's cross section. The observations show that the charge weld rises in the middle of the thickness for each ram speed and billet temperature. However, there is a noticeable pattern difference at the beginning of the charge weld. The findings indicate that the onset of the charge weld is slightly delayed by increased ram speed and decreased billet temperature.

4. Conclusions and outlook

This study focuses on the investigation and prediction of charge weld evolution in AA6060 circular tube extrusion, using combined industrial experimental and advanced numerical modeling approaches. The investigations revolve around the research questions, which need to be addressed: the mechanism of charge weld formation and evolution, the prediction of charge weld evolution and scrap length, and the sensitivity analysis to ram speed and billet temperature. The key findings are summarised as follows:

- The presented analyses reveal the charge weld in the form of identical tongues in the cross section, positioned on both sides of the L-seam welds. Each one is initiated in the middle of the thickness and migrates towards the inner and outer surfaces. Material replacement from the old to the new billet in the cross section starts at a high rate and gradually slows when approaching the transition end.
- The numerical model successfully captures charge evolution across the profile's cross section in the transition zone with remarkably good accuracy, showing errors ranging from 1.5% to 7.5%. Additionally, charge weld scrap length is accurately predicted with less than 1.5% error. However, analytical models identified in the literature systematically underestimate charge weld scrap length. The formula by Saha [25] has an error slightly exceeding 40%, while the formula by Jowett et al. [10] exhibits an error just above 10%.
- Numerical sensitivity analyses show that charge weld length is somewhat sensitive to changes in ram speed, resulting in a relatively smaller dead metal zone and more homogeneous material flow at higher speeds, thus shorter charge welds. However, billet temperature has a negligible effect on charge weld length. Additionally, ram speed and billet temperature slightly affect the onset of charge weld, with higher speeds and lower temperatures delaying its occurrence.

Further work will involve conducting additional experimental analyses to provide robust support for the performed sensitivity analysis of different extrusion parameters. Moreover, a novel charge weld strength prediction model could be developed to optimize the impact of charge weld scrap. Overall, the approaches applied here hold great potential to be extended to address complex shape profile extrusions, leading to broader application of this research in the field.

Consent for publication

This work is original and has not been published elsewhere nor it is currently under consideration for publication elsewhere.

Declaration of Competing Interest

The authors declare that they have no known competing financial interests or personal relationships that could have appeared to influence the work reported in this paper.

Acknowledgements

The authors gratefully acknowledge the financial support from the Norwegian University of Science and Technology (NTNU), NTNU Aluminum Product Innovation Center (NAPIC), and the EXPECT project [No.: 321571] and AluGreen project [No.: 328831] sponsored by Research Council of Norway. In addition, the authors would like to thank Benteler Automotive Raufoss AS (Raufoss, Norway) for the support with extrusion experiments.

References

[1] Bandini C, Reggiani B, Donati L, Tomesani L. Code validation and development of user routines for microstructural prediction with qform. Mater Today: Proc 2015;2 (10):4904–14. https://doi.org/10.1016/j.matpr.2015.10.052.
[2] Biba N, Stebunov S, Vlasov A. May). Application of QForm Program for Improvement of the Die Design and Profile Extrusion Technology. Proc. 9th Int. Al. Extr. Techn. Sem. 2008.
[3] Chen L, Zhao G, Yu J, Zhang W. Evaluation of a pyramid die extrusion for a hollow aluminum profile using FE simulation. J Mech Sci Technol 2015;29(5):2195–203. https://doi.org/10.1007/s12206-015-0440-3.
[4] Cooper DR, Allwood JM. Influence of diffusion mechanisms in aluminium solid-state welding processes. Proc Eng 2014;81:2147–52. https://doi.org/10.1016/j.proeng.2014.10.300.
[5] Den Bakker AJ, Katgerman L, Van Der Zwaag S. Analysis of the structure and resulting mechanical properties of aluminium extrusions containing a charge weld interface. J Mater Process Technol 2016;229:9–21. https://doi.org/10.1016/j.jmatprotec.2015.09.013.
[6] Donati L, Reggiani B, Pelaccia R, Negozio M, Di Donato S. Advancements in extrusion and drawing: a review of the contributes by the ESAFORM community. Int J Mater Form 2022;15(3). https://doi.org/10.1007/s12289-022-01664-w.
[7] Donea J, Huerta A, Ponthot J-Ph, Rodriguez-Ferran A. Arbitrary Lagrangian-Eulerian Methods. In *Encyclopedia of Computational Mechanics*. John Wiley & Sons, Ltd; 2004. https://doi.org/10.1002/0470091355.ecm009.
[8] Duplancic I, Prgin J. Material flow in the extrusion of hollow aluminum sections, through hollow dies. Proc. 4th Int. Al. Extr. Techn. Sem. 1988:235–40.
[9] Hatzenbichler T, Buchmayr B. Finite element method simulation of internal defects in billet-to-billet extrusion. Proc Inst Mech Eng Part B: J Eng Manuf 2010;224(7): 1029–42. https://doi.org/10.1243/09544054JEM1830.
[10] Jowett Chris, Adams Johnie, Daughetee Chris, Lea Greg, Huff OA, Fossl Norm. Scrap allocation. In the Proc of the 9th Extrusion Technol Seminar 2008:223–44.
[11] Levanov AN. Improvement of metal forming processes by means of useful effects of plastic friction. J Mater Process Technol 1997;72(2):314–6. https://doi.org/10.1016/S0924-0136(97)00191-X.
[12] Li Q, Harris C, Jolly MR. Finite element modelling simulation of transverse welding phenomenon in aluminium extrusion process. Mater Des 2003;24(7):493–6. https://doi.org/10.1016/S0261-3069(03)00123-7.
[13] Lou S, Wang A, Lu S, Guo G, Qu C, Su C. Tensile property and micro-texture evolution of the charge weld in a billet-to-billet extrusion of AA6061 aluminum profile. Int J Adv Manuf Technol 2019;103(1–4):1309–23. https://doi.org/10.1007/s00170-019-03573-w.
[14] Loukus A, Subhash G, Imaninejad M. Mechanical properties and microstructural characterization of extrusion welds in AA6082-T4. J Mater Sci 2004;39:6561–9.
[15] Mahmoodkhani Y, Wells MA, Parson N, Poole WJ. Numerical modelling of the material flow during extrusion of aluminium alloys and transverse weld formation. J Mater Process Technol 2014;214(3):688–700. https://doi.org/10.1016/j.jmatprotec.2013.09.028.
[16] Mahmoodkhani Y, Wells M, Parson N, Jowett C, Poole W. Modeling the formation of transverse weld during billet-on-billet extrusion. Materials 2014;7(5):3470–80. https://doi.org/10.3390/ma7053470.
[17] Nanninga N, White C, Mills O, Lukowski J. Effect of specimen orientation and extrusion welds on the fatigue life of an AA6063 alloy. Int J Fatig 2010;32(2): 238–46. https://doi.org/10.1016/j.ijfatigue.2009.06.004.
[18] Nanninga N, White C, Furu T, Anderson O, Dickson R. Effect of orientation and extrusion welds on the fatigue life of an Al-Mg-Si-Mn alloy. Int J Fatig 2008;30(9): 1569–78. https://doi.org/10.1016/j.ijfatigue.2007.11.013.
[19] Negozio M, Pelaccia R, Donati L, Reggiani B, Tomesani L, Pinter T. FEM validation of front end and back end defects evolution in AA6063 and AA6082 aluminum alloys profiles. Proc Manuf 2020;47:202–8. https://doi.org/10.1016/j.promfg.2020.04.178.
[20] Negozio M, Pelaccia R, Donati L, Reggiani B, Pinter T, Tomesani L. Finite element model prediction of charge weld behaviour in AA6082 and AA6063 extruded profiles. J Mater Eng Perform 2021;30(6):4691–9. https://doi.org/10.1007/s11665-021-05752-x.

[21] Oberhausen G, Cooper DR. Modeling the strength of aluminum extrusion transverse welds using the film theory of solid-state welding. SSRN Electr J 2023. https://doi.org/10.2139/ssrn.4488657.
[22] Oberhausen Gregory J, Christopher Anselm AA, Cooper Daniel R. Reducing Aluminum Extrusion Transverse Weld Process Scrap. In: Glenn D, Jian C, Erman T, Anupam V, Yoshinori Y, editors. Forming the Feature. Springer, Cham.; 2021. p. 1003–19. https://doi.org/10.1007/978-3-030-75381-8_84.
[23] Pinter T, Reggiani B, Donati L, Tomesani L. Numerical assessment of the influence of process and geometric parameters on extrusion welds and die deformation after multiple-cycles. Mater Today: Proc 2015;2(10):4856–65. https://doi.org/10.1016/j.matpr.2015.10.034.
[24] Pinter T, Antonios D, Reggiani B, Gamberoni A. Charge Weld Scrap Minimization by Means of Dead Metal Flow Control in Die Design. Extrusion Technology 2016.
[25] Pradip K Saha. Quality Issues of Hollow Extrusions for Aerospace Applications. 9th Extrusion. Technology Seminar; 2008.
[26] QForm U.K. QForm UK Extrusion 10 2022.
[27] Reggiani B, Donati L. Experimental, numerical, and analytical investigations on the charge weld evolution in extruded profiles. Int J Adv Manuf Technol 2018;99(5–8):1379–87. https://doi.org/10.1007/s00170-018-2595-4.
[28] Reggiani B, Pinter T, Donati L. Scrap assessment in direct extrusion. Int J Adv Manuf Technol 2020;107(5–6):2635–47. https://doi.org/10.1007/s00170-020-05127-x.
[29] Saha PK. In aluminum extrusion technology. Alum Extrusion Technol 2000. https://doi.org/10.31399/asm.tb.aet.9781627083362.
[30] Sellars CM, Tegart WJ McG. Hot workability. Int Metall Rev 1972;17(1):1–24. https://doi.org/10.1179/imtlr.1972.17.1.1.
[31] Sheppard T. In extrusion of aluminium alloys. Extrusion Alum Alloys 1999. https://doi.org/10.1007/978-1-4757-3001-2.
[32] Tang J, Chen L, Li Z, Zhao G, Zhang C, Zuo Y. Evolution mechanisms of charge weld during porthole die extrusion of ZK60 Mg profile. J Mater Process Technol 2022;300. https://doi.org/10.1016/j.jmatprotec.2021.117401.
[33] Truong TT, Hsu QC, Tong VC. Effects of solid die types in complex and large-scale aluminum profile extrusion. Appl Sci 2020;10(1). https://doi.org/10.3390/app10010263.
[34] Valberg H. Extrusion welding in aluminium extrusion. Int J Mater Product Technol 2002;17(7):497. https://doi.org/10.1504/IJMPT.2002.001317.
[35] Verlinden B, Suhadi A, Delaey L. A generalized constitutive equation for an AA6060 aluminium alloy. Script Metall Mater 1993;28(11):1441–6. https://doi.org/10.1016/0956-716X(93)90496-F.
[36] Yu J, Zhao G, Chen L. Investigation of interface evolution, microstructure and mechanical properties of solid-state bonding seams in hot extrusion process of aluminum alloy profiles. J Mater Process Technol 2016;230:153–66. https://doi.org/10.1016/j.jmatprotec.2015.11.020.
[37] Yu J, Zhao G, Zhao X, Chen L, Chen M. Microstructures of longitudinal/transverse welds and back-end defects and their influences on the corrosion resistance and mechanical properties of aluminum alloy extrusion profiles. J Mater Process Technol 2019;267:1–16. https://doi.org/10.1016/j.jmatprotec.2018.12.006.
[38] Zener C, Hollomon JH. Effect of strain rate upon plastic flow of steel. J Appl Phys 1944;15(1):22–32. https://doi.org/10.1063/1.1707363.
[39] Zhang C, Dong Y, Wang C, Zhao G, Chen L, Sun W. Evolution of transverse weld during porthole extrusion of AA7N01 hollow profile. J Mater Process Technol 2017;248:103–14. https://doi.org/10.1016/j.jmatprotec.2017.05.017.
[40] Zhao G, Chen H, Zhang C, Guan Y, Anjiang G, Peng L. Die optimization design and experimental study of a large wallboard aluminum alloy profile used for high-speed train. Int J Adv Manuf Technol 2014;74(1–4):539–49. https://doi.org/10.1007/s00170-014-5903-7.